



**HAL**  
open science

# Intracellular Ca<sup>2+</sup> Dynamics in Astrocytes: Modeling the Underlying Spatiotemporal Diversity

Audrey Denizot, Hugues Berry, Sharmila Venugopal

► **To cite this version:**

Audrey Denizot, Hugues Berry, Sharmila Venugopal. Intracellular Ca<sup>2+</sup> Dynamics in Astrocytes: Modeling the Underlying Spatiotemporal Diversity. Encyclopedia of Computational Neuroscience, pp.1-19, inPress. hal-02419317

**HAL Id: hal-02419317**

**<https://inria.hal.science/hal-02419317>**

Submitted on 19 Dec 2019

**HAL** is a multi-disciplinary open access archive for the deposit and dissemination of scientific research documents, whether they are published or not. The documents may come from teaching and research institutions in France or abroad, or from public or private research centers.

L'archive ouverte pluridisciplinaire **HAL**, est destinée au dépôt et à la diffusion de documents scientifiques de niveau recherche, publiés ou non, émanant des établissements d'enseignement et de recherche français ou étrangers, des laboratoires publics ou privés.

# Intracellular $Ca^{2+}$ Dynamics in Astrocytes: Modeling the Underlying Spatiotemporal Diversity

Audrey Denizot<sup>1,2</sup>, Hugues Berry<sup>1,2</sup>, and Sharmila Venugopal <sup>\*3</sup>

<sup>1</sup>INRIA, F-69603, Villeurbanne

<sup>2</sup>Univ Lyon, LIRIS, UMR5205 CNRS, F-69621, Villeurbanne, France

<sup>3</sup>Department of Integrative Biology and Physiology, University of  
California Los Angeles, Los Angeles, CA, USA

## 1 Definition

Astrocytes are a predominant type of glia in the central nervous system. Although they do not generate electrical signals like neurons, they display a form of excitability characterized by fluctuations in their intracellular  $Ca^{2+}$  levels. These  $Ca^{2+}$  fluctuations show remarkable spatiotemporal complexity and diversity and further respond to various cellular stimuli. Modeling astrocyte  $Ca^{2+}$  dynamics is an essential step towards understanding their physiology and functions within neural circuits. This article highlights the computational methods and approaches for modeling intracellular  $Ca^{2+}$  signals in astrocytes at the single cell level.

## 2 Detailed Description

Astrocytes are ubiquitously distributed throughout the central nervous system. Each astrocyte can display a complex morphology characterized by distinct compartments: the soma, primary branches and numerous fine processes, also referred to as branchlets. The latter account for around 75% of the surface of the astrocytic plasma membrane [1], providing astrocytes a spongiform appearance (see Fig 1). Some of the fine processes, referred to as perisynaptic processes (PAPs), are in apposition to pre- and post- synaptic neurons, forming tripartite synapses, where they might modulate neuronal communication (see e.g Savtchouk et al. 2018 [2] for a review). Some astrocytic ramifications, referred to as endfeet, wrap around blood vessels and are involved in neurovascular

---

\*Email: vsharmila@g.ucla.edu

coupling. Astrocytes also regulate neuronal excitability by maintaining ionic homeostasis (e.g.  $K^+$  buffering), uptaking neurotransmitters and moderating synaptogenesis [3].

19  
20  
21  
22

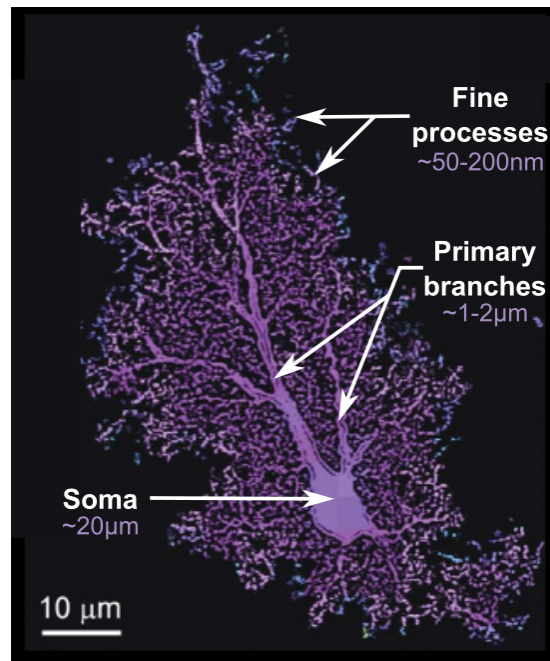


Figure 1: **Astrocytes are characterized by a complex morphology.** Confocal image of a dye-filled hippocampal astrocyte, revealing its spongiform structure. Numbers in purple correspond to the approximate diameter of the different cellular compartments observed: the cellular body (soma), primary branches and fine processes. Adapted from Shigetomi et al. 2013 [4].

## 2.1 Diversity of astrocyte $Ca^{2+}$ signals

23

Cytosolic  $Ca^{2+}$  levels in astrocytes show ongoing fluctuations, both *in vitro* and *in vivo* [3]. The amplitude, duration and frequencies of these so-called  $Ca^{2+}$  signals/events vary depending on stimuli, such as Adenosine-triphosphate (ATP) and glutamate. As such, those  $Ca^{2+}$  signals are crucial reporters of astrocyte function and are therefore a widely accepted form of astrocyte excitability. Astrocyte  $Ca^{2+}$  signals can result from diverse mechanisms such as  $Ca^{2+}$  influx from channels on the membrane of intracellular stores or on the plasma membrane, the spatial distribution of these channels, ATP signaling and inter-cellular propagation of  $Ca^{2+}$  via gap junction coupling between astrocytes [5]. A major pathway that triggers the release of  $Ca^{2+}$  in astrocytes is initiated by agonists binding to transmembrane G-protein-coupled receptors (GPCRs). This activates the synthesis of an intracellular second messenger, Inositol 3-Phosphate ( $IP_3$ ).

24  
25  
26  
27  
28  
29  
30  
31  
32  
33  
34

The  $IP_3$  molecules bind to  $IP_3$  receptor channels (IP3Rs), located on the endoplasmic reticulum (ER) membrane. Binding of  $IP_3$  and  $Ca^{2+}$  to IP3Rs leads to the opening of IP3Rs, resulting in a  $Ca^{2+}$  influx from the ER into the cytosol. The resulting local increase in  $Ca^{2+}$  concentration, together with the  $IP_3$  molecules, further activates more IP3R channels. This positive feedback loop, referred to as  $Ca^{2+}$ -induced- $Ca^{2+}$  release (CICR) can combine with the diffusion of  $Ca^{2+}$  and  $IP_3$  to result in the propagation of  $Ca^{2+}$  events in the form of waves and of global (whole-cell) events.  $Ca^{2+}$  diffusion as well as pumps then restore basal cytosolic  $Ca^{2+}$  levels, thus terminating the signals.

The recent use of super-resolution microscopy and of highly sensitive genetically encoded  $Ca^{2+}$  indicators (GECIs) have revealed striking spatiotemporal diversity of astrocyte  $Ca^{2+}$  signals. Notably, there are remarkable differences between signals in the soma and in the peripheral processes [6] (see Fig 2). The latter account for around 80% of the total astrocytic  $Ca^{2+}$  activity *in vivo* [1]. Those signals are localized in so-called microdomains and display faster kinetics and an order of magnitude smaller amplitudes compared to somatic  $Ca^{2+}$  signals. Around half of  $Ca^{2+}$  signals in fine processes persist in the absence of type 2  $IP_3$ Rs. The  $Ca^{2+}$  pathways responsible for the other half of  $Ca^{2+}$  signals in branchlets are currently unknown and could involve type 1 or 3  $IP_3$ Rs,  $Ca^{2+}$  channels on the plasma membrane or on the membrane of internal stores.

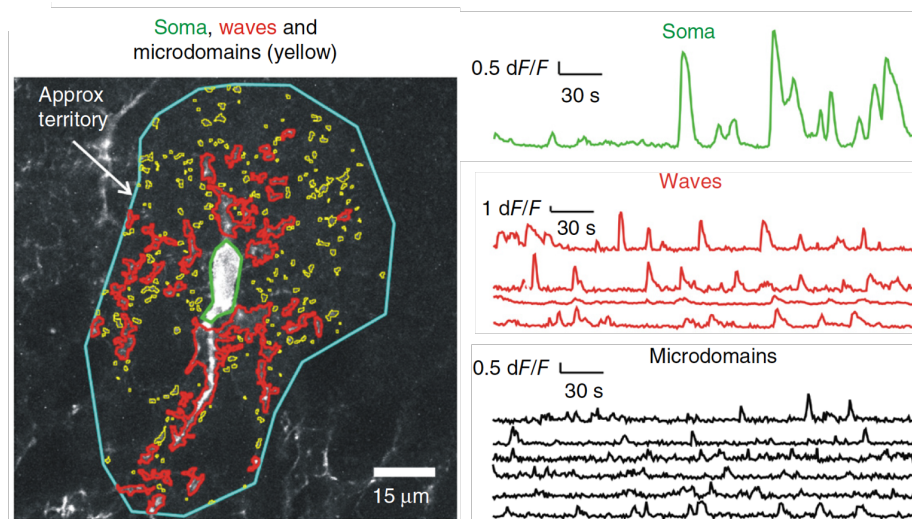


Figure 2: **Diversity of astrocyte intracellular  $Ca^{2+}$  signals.** *Left:* Astrocyte  $Ca^{2+}$  signals in a hippocampal astrocyte reported by GCaMP6f can be detected in discrete cellular compartments. The blue contour demarcates the approximate boundary of the anatomical domain of the astrocyte. *Right:* The detected signals consist of large amplitude somatic oscillations (green), waves, largely in primary branches (red) and microdomains in fine processes (black traces, corresponding to yellow regions in the left image). Adapted from Srinivasan et al. 2015 [6] with permission.

A summary of the different spatial patterns of astrocytic  $Ca^{2+}$  signals is shown in Fig 3 and their key features are listed below. 56 57

- **Global signals** (Fig 3A) are  $IP_3R$ -dependent  $Ca^{2+}$  signals that propagate within the whole astrocyte [1]. 58 59
- **Local waves** (Fig 3B) are observed in branches and sporadically propagate bidirectionally to and from the soma.  $Ca^{2+}$  signals could also propagate through gap junction coupling between processes from the same cell [7] (Fig 3E), although this has not been reported so far. Note that gap junction coupling also allows for the propagation of intercellular waves, which will not be discussed here as this work focuses on  $Ca^{2+}$  signals at the single-cell level (see e.g. Giaume et al. 1998 [8] for a review). 60 61 62 63 64 65 66
- **Spatially restricted microdomains** (Fig 3C-D) are non-propagating signals characterized by distinct temporal properties (with a signal duration from the order of seconds [6] to tens of seconds [9]) and can be mediated by Tetrodotoxin (TTX)-sensitive (neuronal activity-dependent) and TTX-resistant mechanisms. Furthermore, these events can occur as  $IP_3R$ -independent events, notably in the absence of somatic  $Ca^{2+}$  signals [6]. Those signals are mostly observed in perisynaptic processes (Fig 3C) or in blood vessel-associated endfeet (Fig 3D) [1]. 67 68 69 70 71 72 73

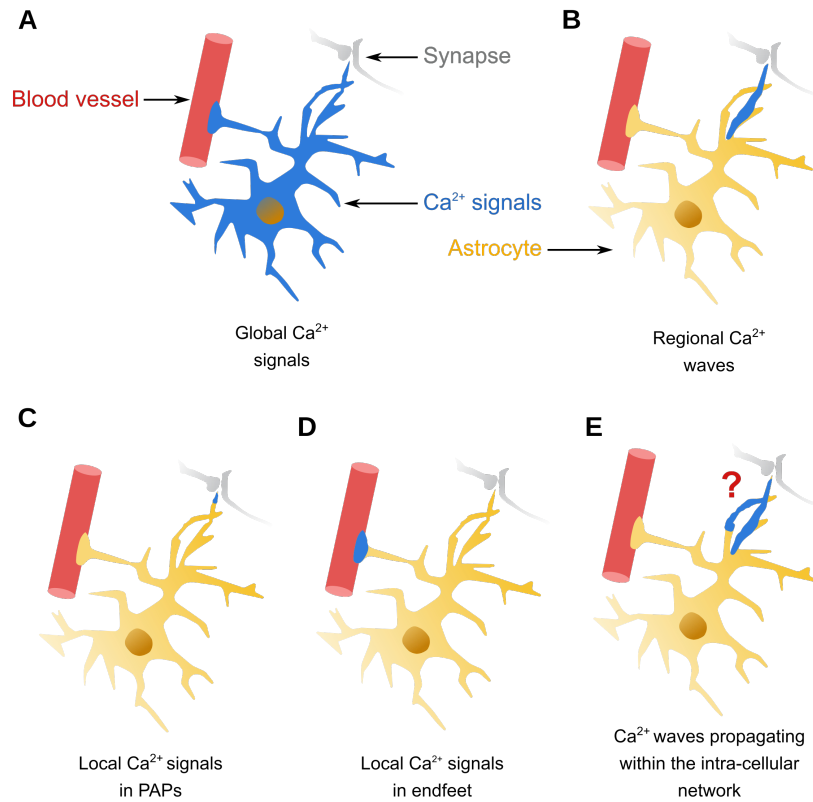


Figure 3: **Spatial diversity of intracellular  $Ca^{2+}$  signals in astrocytes.**  $Ca^{2+}$  signals in a single astrocyte display various spatial forms. Some signals can propagate within the whole cell, forming a global event (A), propagate via regionalized  $Ca^{2+}$  waves (B) or can be localized at the vicinity of synapses (C), in endfeet (D), or might propagate to other processes of the same cell via gap junctions, although such an intracellular propagation via gap junction coupling has not been reported yet (E). PAP: Perisynaptic astrocytic process.

Taken together, the diversity of intracellular astrocyte  $Ca^{2+}$  signals concerns their spatial extent (from localized microdomains to whole-cell events), their time-scales (order of seconds to tens of seconds) and, arguably, the mechanisms which trigger them. Their physiological roles are not well understood and constitute an active area of research (e.g., see review [3]). It is likely that the observed spatiotemporal variability of astrocyte  $Ca^{2+}$  signals is associated with the integration of signals in neural circuits coupled to local blood flow changes and metabolic processes to orchestrate integrative physiological functions.

74  
75  
76  
77  
78  
79  
80  
81  
82

## 2.2 Modeling Astrocyte $Ca^{2+}$ Dynamics

The apparent diversity of intracellular astrocyte  $Ca^{2+}$  signals has led to the development of advanced computational tools and approaches to model astrocyte  $Ca^{2+}$  dynamics. A recent and significant advance corresponds to the development of spatially-explicit multi-compartment models with realistic 3D morphologies in order to fully reproduce the spatiotemporal diversity of astrocyte  $Ca^{2+}$  signals (for a detailed review, see Manninen et al. 2018 [10]).

### 2.2.1 Approaches for modeling astrocyte $Ca^{2+}$ dynamics

In this section, the different approaches that can be used for simulating astrocyte  $Ca^{2+}$  signals are presented. Fig 4A summarizes those approaches, the approximations associated to it as well as the resulting computational cost and accuracy. Briefly, modeling approaches can be deterministic, i.e in which all future states can be determined from the current state, or stochastic, i.e considering each reaction as a probabilistic event. They can also be well-mixed, i.e considering space as homogeneous and assuming that molecules are equally distributed within the system, or spatially-explicit. Those methods can be coupled within hybrid models (see e.g. Winkelmann et al. 2017 [11] for a review).

The first models of astrocyte  $Ca^{2+}$  signals were deterministic and well-mixed, formulated with ordinary differential equations (ODEs) [10]. Those models offered crucial insights on the qualitative and quantitative behaviors of the observed dynamics. However, the probabilistic molecular interactions in reaction-diffusion systems often necessitate stochastic modeling approaches. Moreover, the spatial complexity of astrocyte morphology and  $Ca^{2+}$  signals (see Fig 1 and 2) has led to the development of spatially-explicit models. Fig 4B presents the different geometries that can be used in spatially-explicit models of astrocyte  $Ca^{2+}$  signals. They can be either realistic or simplified, in 1-3 spatial dimensions. Those models are more realistic, increasing the accuracy of model predictions, however associated with an increased computational cost.

As fine astrocytic processes display complex geometries and have small volumes with low copy number of molecules, models of  $Ca^{2+}$  signals at this spatial scale are both stochastic and spatially-explicit. The three main spatially-explicit stochastic approaches used for simulating reaction-diffusion systems are presented in Fig 4C and a brief summary is also provided below. An excellent review of these approaches can be found in Burrage et al. 2011 [12] and **CrossRef: Stochastic Simulators, Particle-Based Stochastic Simulators** detail the available spatially-explicit stochastic simulators.

- **Particle-based (or particle-tracking or microscopic) models** ( Fig 4C1)

The most straightforward stochastic spatially-explicit approach consists of tracking the diffusive path of each individual molecule/ion (referred to as particle) within the spatial domain. Particles are characterized by their individual spheres of interaction/interaction radii. Second-order reactions occur depending on their rates when the reactants are within their interaction radii.

- **Voxel-based (or population-based or mesoscopic) models** ( Fig 4C2) 125  
As they are less computationally expensive than particle-based approaches, most 126  
intracellular  $Ca^{2+}$  models are implemented with the voxel-based stochastic ap- 127  
proach. In this approach, the spatial domain is divided into small compartments 128  
(voxels) that are assumed well-mixed and reactions can occur between reactants 129  
within the same voxel. Diffusion is modeled as a reaction in which the number 130  
of molecules in the origin compartment is decreased by one while the number of 131  
molecules in the neighboring compartment is increased by one. Accuracy and 132  
computational cost decrease with increasing sizes of compartments. (**Cross-Ref:** 133  
**Stochastic Simulators**). 134
- **Hybrid models** (Fig 4C3) 135  
Hybrid methods describe regions of particular interest such as the vicinity of 136  
 $Ca^{2+}$  channels with microscopic details while other regions are simulated with 137  
a compartment-based approach. Those methods thus offer a trade-off between 138  
detailed modeling and computational cost. 139



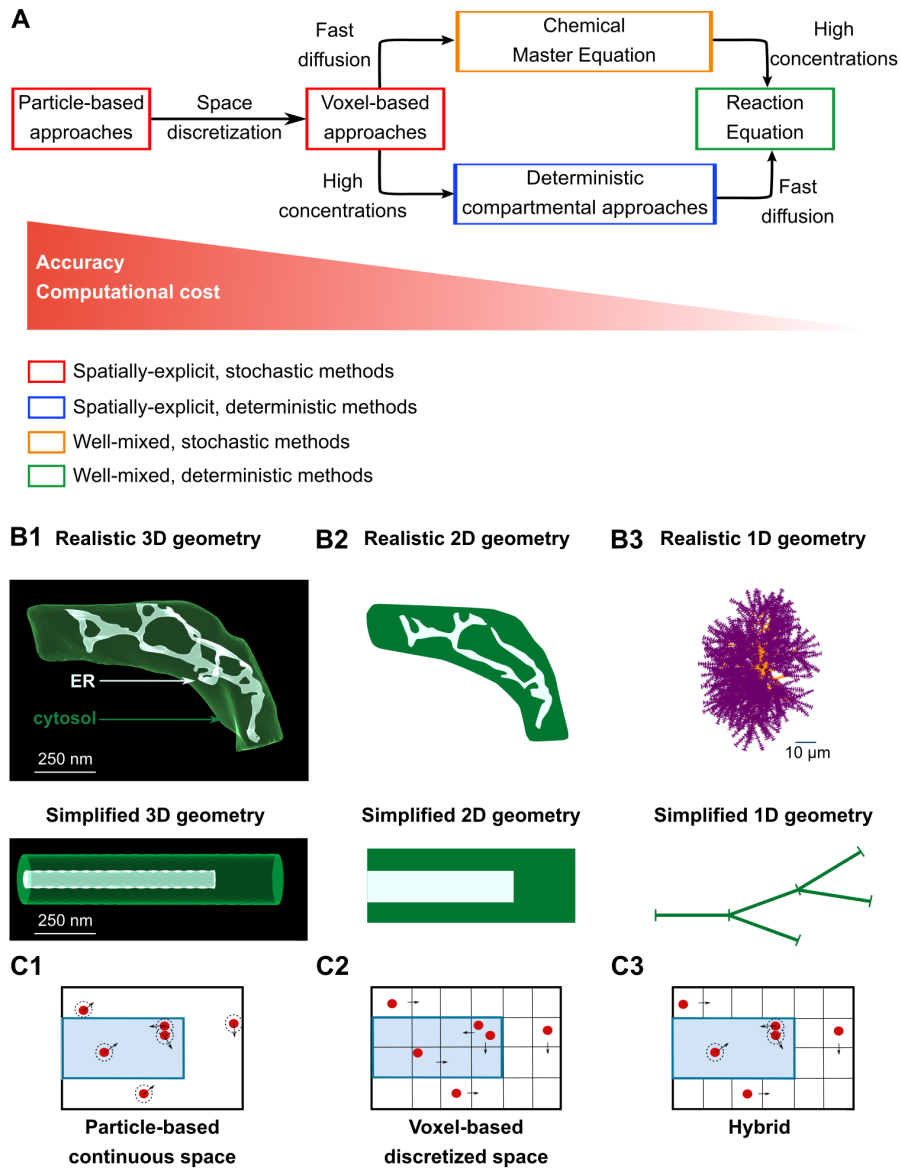


Figure 4: **Approaches for modeling intracellular  $Ca^{2+}$  signals in astrocytes.** (A) The different approaches available for modeling  $Ca^{2+}$  signals are presented from high accuracy/high computational cost associated with Brownian dynamics to less accurate but faster models of reactions based on ordinary differential equations. Note that hybrid methods are not represented in this schematic. (B) Depending on the biological question, the astrocytic geometry chosen for simulations can be in 3D (B1), either realistic, extracted from 3D reconstructions of experimental data (top) or simplified (bottom). The mesh in top B1 panel corresponds to a hippocampal astrocytic process extracted and reconstructed from electron microscopy, provided by C. Calì, BESE Division, King Abdullah University of Science and Technology, Thuwal, Saudi Arabia [13].

Figure 4: **Approaches for modeling intracellular  $Ca^{2+}$  signals in astrocytes (continued)**. Cytosolic volume is represented in green and ER volume in blue. 2D (B2) or 1D (B3) projections of 3D geometries can also be performed for computational efficiency, although it decreases the accuracy of the model. The top B3 panel was taken from Savtchenko et al. 2018 [14], with permission. Panel C presents the main strategies for performing spatially-explicit stochastic simulations: Particle-based (C1), Voxel-based (C2) and Hybrid (C3) approaches.

### 2.2.2 Deterministic models of $Ca^{2+}$ oscillations in astrocytes

The early mathematical models of astrocyte  $Ca^{2+}$  signals primarily simulated the dynamics of  $IP_3$ -dependent  $Ca^{2+}$  release from the ER. These largely consisted of deterministic models based on ODEs. The positive feedback loop of the CICR mechanism consisted of the rate of cytosolic  $Ca^{2+}$  influx as a sigmoid or Hill function of  $IP_3$  concentration (see [15] for a review). The termination of the resulting cytosolic  $Ca^{2+}$  increase resulted from the re-uptake of  $Ca^{2+}$  into the ER via the activity of Smooth Endoplasmic Calcium ATPases (SERCA) pumps and from the exponential decay of  $IP_3$  concentration. Together, the CICR and SERCA mechanisms formed the basis for oscillatory models of  $Ca^{2+}$  dynamics (see Fig 5). Influx of  $Ca^{2+}$  via transmembrane voltage-gated  $Ca^{2+}$  channels was also incorporated using constant rates or realistic conductance-based (Hodgkin-Huxley) formalism.

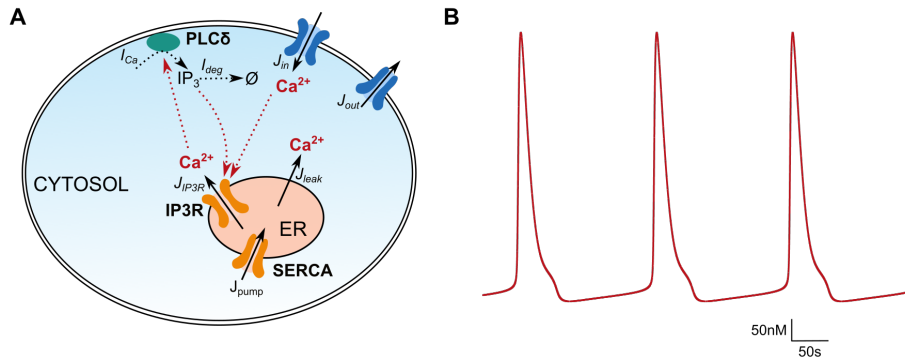


Figure 5: **Classic  $IP_3$ -dependent pathway incorporated in models of intracellular  $Ca^{2+}$  oscillations in astrocytes.** (A) The schematic shows typical sources of astrocyte  $Ca^{2+}$  incorporated in models (see Table 1 for a description of the various terms and Eq 1 for the ODE formulation of the system). Note that the pathway presented here is simplified, see De Pitta et al. 2019 [15] and Dupont et al. 2016 [16] for further details. (B) A simulated trace of intracellular  $[Ca^{2+}]$ , displaying  $[Ca^{2+}]$  oscillations, based on the model from Lavrentovich et al. 2008 [17].

Table 1: Description of terms shown in Fig 5 and 6.

| <b><math>Ca^{2+}</math> dynamics</b> |   |
|--------------------------------------|---|
| $J_{IP3}$                            | $Ca^{2+}$ influx from the ER to the cytosol through open IP3R |
| $J_{in}$                             | $Ca^{2+}$ leak from the extracellular space to the cytosol    |
| $J_{out}$                            | $Ca^{2+}$ outflux from the cytosol to the extracellular space |
| $J_{leak}$                           | $Ca^{2+}$ leak from the ER to the cytosol                     |
| $J_{pump}$                           | $Ca^{2+}$ uptake from the cytosol to the ER by SERCA pumps    |
| $J_{Glu}$                            | Glutamate-evoked $Ca^{2+}$ influx                             |
| $J_{diff}$                           | Cytosolic $Ca^{2+}$ diffusion                                 |
| $D_{Ca}$                             | $Ca^{2+}$ coefficient of diffusion                            |
| $[Ca^{2+}]_c$                        | Cytosolic $Ca^{2+}$ concentration                             |
| $[Ca^{2+}]_{ER}$                     | ER $Ca^{2+}$ concentration                                    |
| <b><math>IP_3</math> dynamics</b>    |   |
| $I_{Glu}$                            | Glutamate-evoked $IP_3$ production by PLC $\beta$             |
| $I_{Ca}$                             | $Ca^{2+}$ -dependent $IP_3$ production by PLC $\delta$        |
| $I_{deg}$                            | $IP_3$ degradation term                                       |
| $I_{Diff}$                           | Cytosolic $IP_3$ diffusion                                    |
| $[IP_3]$                             | Cytosolic $IP_3$ concentration                                |
| <b>Glutamate dynamics</b>            |   |
| $\xi_p(t)$                           | Stochastic glutamate source (Poisson process)                 |
| $\tau_{glu}$                         | Synaptic glutamate decay rate constant                        |
| $G_{Diff}$                           | Glutamate diffusion in the extracellular space                |
| $[Glu]$                              | Extracellular glutamate concentration                         |
| $[Glu]^*$                            | Extracellular glutamate concentration at steady state         |
| <b>Other parameters</b>              |   |
| $c_1$                                | Ratio between ER and cytosolic volumes                        |

$$\begin{aligned}
 \frac{d[Ca^{2+}]_c}{dt} &= J_{IP3} + J_{leak} - J_{pump} + J_{in} - J_{out} \\
 \frac{d[Ca^{2+}]_{ER}}{dt} &= \frac{1}{c_1} (J_{pump} - J_{leak} - J_{IP3}) \\
 \frac{d[IP_3]}{dt} &= I_{Ca} - I_{deg}
 \end{aligned} \tag{1}$$

To segregate the distal (peripheral)  $Ca^{2+}$  microdomains from somatic events, deterministic models have incorporated spatial partitioning based on realistic astrocyte morphology. The Brazhe et al. 2018 [18] model, for instance, considered the z-projection of the 3D morphology of a rodent hippocampal astrocyte (see Fig 6A). Following a spatial discretization, the internal compartments were labelled as belonging either to the perimembrane region (type-I) or the deep region (type-II), depending on their distance from plasma membrane. In type-I regions, glutamate binding at synapses can promote  $IP_3$  production and  $Ca^{2+}$  influx. Local  $Ca^{2+}$  increases and concomitant  $IP_3$

production were posited to spatially diffuse into the neighboring type-II region. The 161  
type-II region consisted of the classic  $IP_3$ R-activated  $Ca^{2+}$  release from the ER and the 162  
 $IP_3$ - $Ca^{2+}$  CICR, together capable of generating global waves via a positive feedback 163  
loop. The two regions were assumed to be coupled by a diffusive  $Ca^{2+}$  flux ( $J_{diff}$ ) 164  
and an  $IP_3$  flux ( $I_{diff}$ ) for which the diffusion coefficients were estimated based on the 165  
cell morphology. This approach offers insight into a mechanism by which synaptically 166  
driven peripheral  $Ca^{2+}$  fluctuations might contribute to the integration and initiation 167  
of global events (see Fig 6B). Additionally, modeling the synaptic input with a noise 168  
term (e.g. Poisson process) generated uncorrelated peripheral events representative of 169  
realistic  $Ca^{2+}$  microdomains. An advantage of this model is that it can be used to study 170  
signal propagation within ER-free branchlets. 171

172

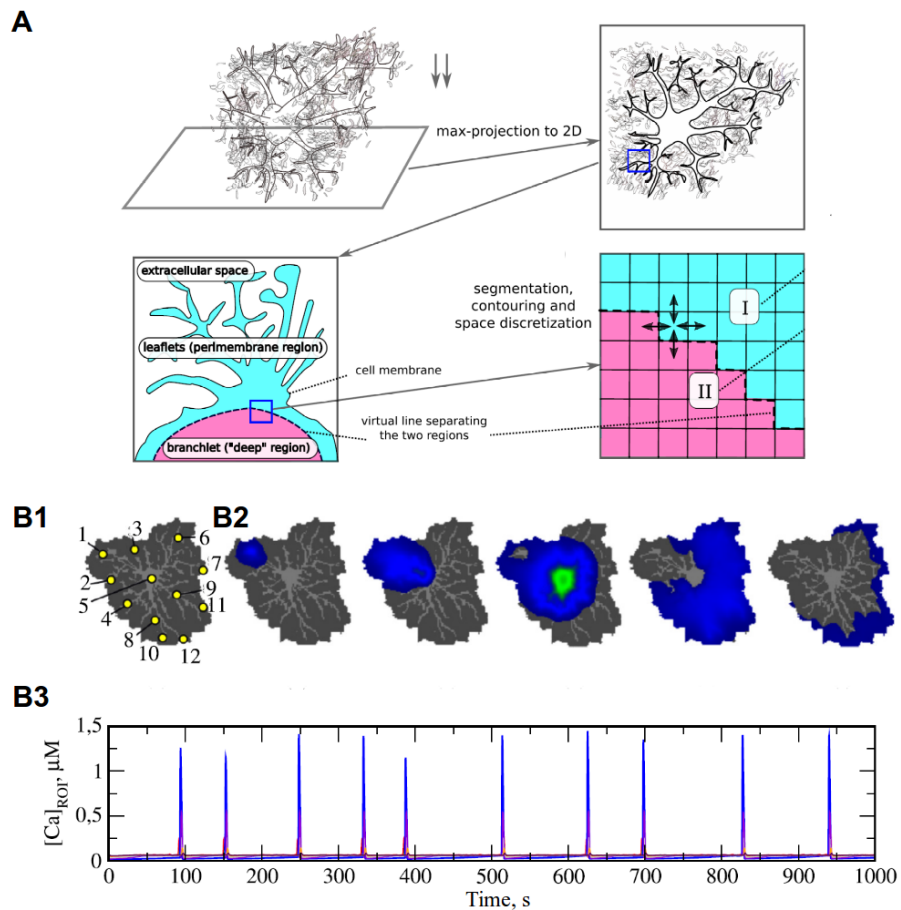


Figure 6: **Spatially partitioned oscillators.** (A) 3D reconstruction from an astrocyte imaged with confocal fluorescent microscopy was projected in 2D and then divided into 2 types of compartments: perimembrane (blue) or deeper regions (pink), that were then spatially discretized. The ODEs that describe  $Ca^{2+}$  and  $IP_3$  dynamics in both compartments are presented in Eq 2 and 3. Terms are described in Table 1. (B1) Image displaying the different regions of interest (ROIs) within the model (numbered 1 - 12). (B2) Snapshots of a single  $Ca^{2+}$  wave originating at ROI 1. (B3) Time series of all the ROIs. For a detailed figure legend, see [18]. Adapted from Brazhe et al. 2018 [18] with permission from authors and AIP Publishing LLC.

ODEs for the perimembrane, glutamate uptake-dependent, region from the Brazhe 173

et al model [18] (Type I region, see Fig 6A, blue):

174

$$\begin{aligned}
 \frac{d[Ca^{2+}]_c}{dt} &= J_{in} + J_{glu} - J_{out} + J_{diff} \\
 \frac{d[Glu]}{dt} &= \frac{[Glu]^* - [Glu]}{\tau_{Glu}} + \xi_p + G_{diff} \\
 \frac{d[IP_3]}{dt} &= I_{Glu} + I_{Ca} - I_{deg} + I_{diff}
 \end{aligned} \tag{2}$$

ODEs for the deep,  $IP_3$ R activation-dependent, region from the Brazhe et al model [18] (Type II region, see Fig 6A, pink):

175

176

$$\begin{aligned}
 \frac{d[Ca^{2+}]_c}{dt} &= J_{IP3} + J_{leak} - J_{pump} + J_{diff} \\
 \frac{d[Ca^{2+}]_{ER}}{dt} &= -\frac{1}{c_1}(J_{IP3} + J_{leak} - J_{pump}) \\
 \frac{d[IP_3]}{dt} &= I_{diff} - I_{deg}
 \end{aligned} \tag{3}$$

Recently, detailed 3D reconstructions of astrocyte morphology have been used to generate realistic spatially-explicit compartmental models of astrocytes combined with deterministic formulation of  $Ca^{2+}$  fluxes within compartments [14] (see Fig 7A). The spatial discretization has captured the spatiotemporal dynamics of diverse  $Ca^{2+}$  signals measured experimentally, supporting the usefulness of this approach to further investigate astrocyte physiology in health and disease. However, molecular reactions in small discrete compartments such as microdomains in fine astrocytic processes are inherently probabilistic events. Stochastic modeling approaches offer an attractive alternative when a detailed description of  $Ca^{2+}$  signals in microdomains is needed.

177

178

179

180

181

182

183

184

185

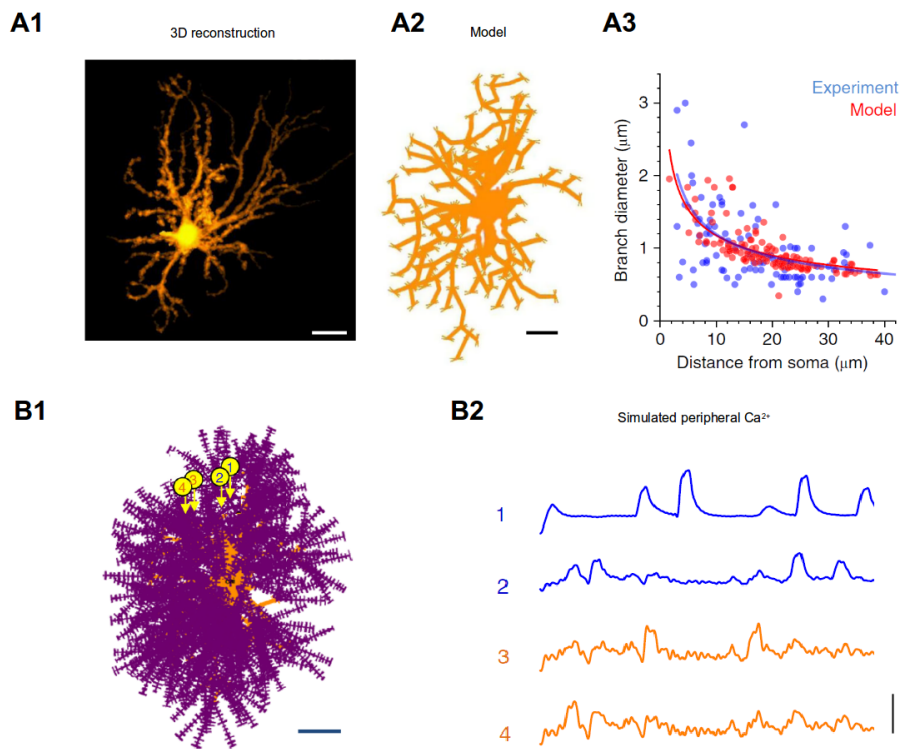


Figure 7: **Astrocyte model with realistic 3D morphology.** (A1) 3D reconstructed stem tree of an astrocyte from the hippocampal CA1 region. Scale bar, 10  $\mu\text{m}$ . (A2) A typical astrocyte stem tree in NEURON format. Scale bar, 10  $\mu\text{m}$ . (A3) Comparison of branch diameters in the model (red) and in experiments (blue). Solid lines are best-fit dependence using power law for the corresponding data scatters. (B1) A complete astrocyte morphology model (z-projection) generated in the NEURON modeling software. The main branches and the nanoscopic processes are depicted in orange and purple, respectively. Scale bar, 10  $\mu\text{m}$ . (B2) Time series of simulated intracellular  $Ca^{2+}$  dynamics in the ROIs labeled 1-4 in the morphology shown on the left panel. Scale bars (v, h): 100%  $\Delta F/F$ , 20s. See [14] for detailed figure legends. Reproduced from Savtchenko et al. 2018 [14] with author permission; article with Creative Commons License.

### 2.2.3 Stochastic approaches for modeling intracellular astrocyte $Ca^{2+}$ signals

186

Molecular interactions in spatially-restricted compartments such as thin astrocytic processes, which are believed to be the site of neuron-astrocyte communication, occur when molecules are in low copy numbers. Stochastic approaches can describe the associated heterogeneous reaction rates and the inherent stochasticity of biochemical reactions so that they are being used to model astrocyte  $Ca^{2+}$  signals in fine processes.

187

188

189

190

191

192 Recently, some astrocyte models have started to incorporate noise using hybrid ap- 193  
194 proaches in order to better simulate stochastic components of  $Ca^{2+}$  dynamics at the 195  
196 subcellular level. For example, Cresswell-Clay et al. 2018 [19] have developed a 197  
198 whole-cell model of a single astrocyte consisting in a soma with 5 main branches, all 199  
200 containing ER.  $Ca^{2+}$  signals were implemented as a stochastic influx. Their results 201  
202 suggest that both cellular geometry (e.g somatic volume) and the velocity of diffusing 203  
204 molecules influence the coupling and nature of the  $Ca^{2+}$  signals in response to neuronal 205  
206 stimulation. Interestingly, simulations also revealed complex spatiotemporal character- 207  
208 istics of  $Ca^{2+}$  depletion in the somatic ER in response to  $Ca^{2+}$  signals in processes, 209  
210 due to intra-ER  $Ca^{2+}$  diffusion. For reviews on stochastic models of  $Ca^{2+}$  signals, see 211  
212 e.g Rudiger et al. 2019 [20] and Manninen et al. 2018 [10] for astrocytes. 213

214 As the nanoscale geometry of astrocytic processes can reduce diffusion coefficients 215  
216 due to the tortuosity of the compartment, accurate description of the local variations of 217  
218 the number of  $Ca^{2+}$  ions requires spatially-explicit models. Spatially-explicit stochas- 219  
220 tic models of  $Ca^{2+}$  signaling were first developed to reproduce local  $Ca^{2+}$  dynamics 221  
222 in neural dendrites, characterized by small volumes and low numbers of  $Ca^{2+}$  ions 223  
224 (5-6 ions in a half- $\mu\text{m}$  diameter dendritic spine). These studies have demonstrated 225  
226 the influence of dendritic morphology (e.g. dendritic diameter) on the spatiotemporal 227  
228 characteristics of  $Ca^{2+}$  signals and their compartmentalization (see **CrossRef: Cal- 229  
230 cium Dynamics in Neuronal Microdomains: Modeling, Stochastic Simulations, 231  
232 and Data Analysis**). These models highlighted the influence of diffusive noise on 233  
234 intracellular signaling networks, suggesting that noise is an important factor to be con- 235  
236 sidered for accurate description of molecular interactions. 237  
238 A novel spatially-explicit fully stochastic model of  $Ca^{2+}$  signals in astrocytes has been 239  
240 proposed by Denizot et al. 2019 [21]. The two types of spatially-explicit stochastic 241  
242 implementations in the study were: 243

- 244 • A 2D particle-based model to explore the effects of model parameters on the 245  
246 range of  $Ca^{2+}$  dynamics that the model can display. 247
- 248 • A 3D voxel-based model in which the geometry of the reaction volume mim- 249  
250 icking an astrocytic process consisted of a cylinder of length  $L_{\text{astro}}=1 \mu\text{m}$  and 251  
252 radius  $R_{\text{astro}}=0.1 \mu\text{m}$  (Fig 8B). Several variations of this model have been im- 253  
254 plemented to investigate the effects of multiple mechanisms on astrocyte  $Ca^{2+}$  255  
256 microdomains including: 1) clustering of  $IP_3R$  channels, 2) endogenous buffers, 257  
258 and 3) GCaMPs (ultrasensitive genetically-encoded  $Ca^{2+}$  indicators that fluo- 259  
260 resce when bound to  $Ca^{2+}$ ). 261

262  $Ca^{2+}$  dynamics in simulations of the model were compared to signals that were mea- 263  
264 sured experimentally in fine processes of hippocampal astrocytes (Fig 8A). The model 265  
266 successfully reproduced  $Ca^{2+}$  peak amplitude, frequency and duration measured in fine 267  
268 processes and is therefore a valuable tool for investigating intracellular astrocytic  $Ca^{2+}$  269  
270 signals at the subcellular level. Key insights from this model highlight the importance 271  
272 of the spatial distribution of various  $Ca^{2+}$  sources within an astrocyte and suggest that 273  
274 local variations of  $Ca^{2+}$  indicators might contribute to the spatiotemporal diversity of 275  
276 astrocytic  $Ca^{2+}$  excitability. 277



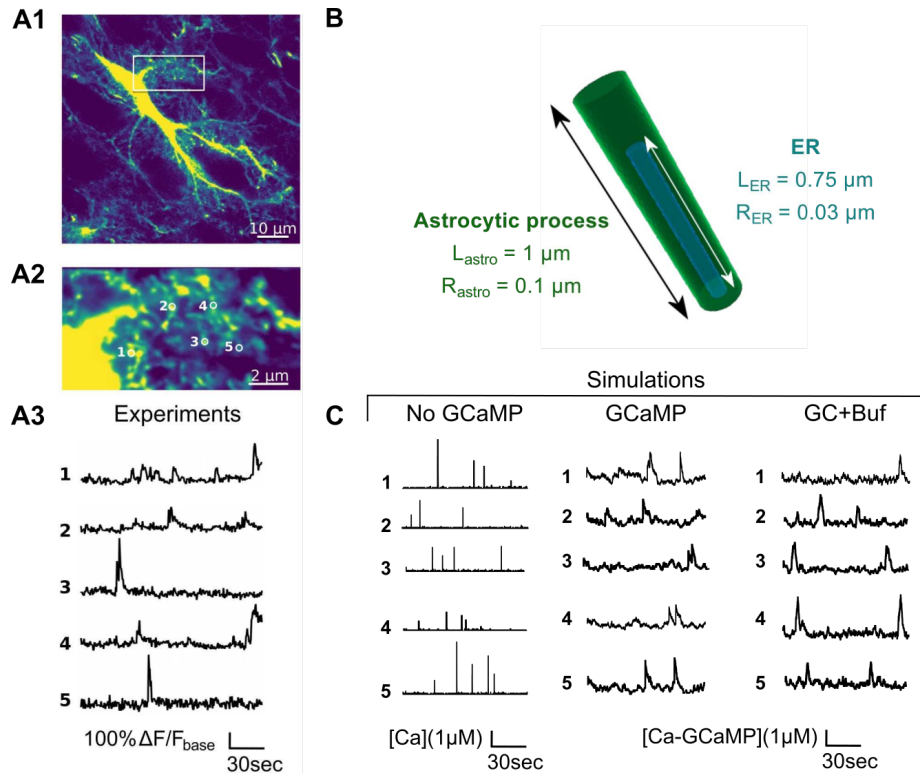


Figure 8: **Simulations of a fully stochastic voxel-based model reproduce experimental measurements of  $Ca^{2+}$  signals in fine astrocytic processes.** (A1) Spontaneous local  $Ca^{2+}$  signals were measured in GCaMP6s-expressing astrocytes from hippocampal organotypic culture. (A2) Magnification of panel A1, presenting the 5 regions of interest (1-5) from which  $Ca^{2+}$  traces have been recorded (A3). (B) Geometry used in simulations that represents a simplified region of interest, i.e a fine process. It consists in a cylinder that is  $1 \mu\text{m}$  long and  $200 \text{ nm}$  in diameter. (C) Representative simulations of  $Ca^{2+}$  dynamics within the fine process geometry presented in panel B, with the different implementations of the model: “No-GCaMP” (no buffers are present in the model, free  $Ca^{2+}$  concentration is monitored), “GCaMP” (GCaMP  $Ca^{2+}$  indicators are added to the model, GCaMP- $Ca$  concentration is monitored) and “GC+Buf” (GCaMP and endogenous  $Ca^{2+}$  buffers are added to the model, GCaMP- $Ca$  concentration is monitored). Adapted from Denizot et al. 2019 [21] with permission, article with Creative Commons License.

### 2.3 Conclusion

Understanding astrocytic  $Ca^{2+}$  signaling is at the forefront of neuroscience research. The diversity of astrocyte  $Ca^{2+}$  excitability may relay spatiotemporally complex code which yet remains to be decoded. Computational modeling of astrocyte physiology and  $Ca^{2+}$  dynamics is an essential step towards unravelling the functions of astrocytes in

236

237

238

239

240

neural circuits. Recent conceptual advances in experimental work have highlighted the spatiotemporal diversity of  $Ca^{2+}$  signals at the single-cell level. Parallel advances in tools and methods for modeling astrocytes are beginning to provide novel insights into their physiology. Future work combining neuron-astrocyte models may thus enhance our understanding of the role of astrocytes in neural signal processing in health and disease.

### 3 Cross-References

|  |     |
|--|-----|
| - Astrocytes $Ca^{2+}$ signaling   | 248 |
| - Astrocyte $Ca^{2+}$ Signals and Their Analysis   | 249 |
| - Neuron-Glial Interactions  | 250 |
| - Models of $Ca^{2+}$ signaling  | 251 |
| - Biochemical Signaling Pathways and Diffusion: Overview   | 252 |
| - $Ca^{2+}$ Release, Models of   | 253 |
| - Modeling Ion Concentrations  | 254 |
| - Signaling Pathways, Modeling of  | 255 |
| - Markov models of ion channels  | 256 |
| - Calcium Dynamics in Neuronal Microdomains: Modeling, Stochastic Simulations, and Data Analysis | 257 |
| - Spatial modeling   | 259 |
| - Deterministic Reaction-Diffusion Simulators  | 260 |
| - Particle-Based Stochastic Simulators   | 261 |
| - Spatial stochastic simulators  | 262 |
| - STEPS: STochastic Engine for Pathway Simulation  | 263 |
| - MCell  | 264 |
| - Stochastic simulators  | 265 |

### References

|   |                                 |
|---|---------------------------------|
| [1] E. Bindocci, I. Savtchouk, N. Liaudet, D. Becker, G. Carriero, and A. Volterra, “Three-dimensional $Ca^{2+}$ imaging advances understanding of astrocyte biology,” <i>Science</i> , vol. 356, p. eaai8185, May 2017.  | 268<br>269<br>270               |
| [2] I. Savtchouk and A. Volterra, “Gliotransmission: Beyond Black-and-White,” <i>Journal of Neuroscience</i> , vol. 38, pp. 14–25, Jan. 2018.   | 271<br>272                      |
| [3] A. Verkhratsky and M. Nedergaard, “Physiology of Astroglia,” <i>Physiological Reviews</i> , vol. 98, pp. 239–389, Jan. 2018.  | 273<br>274                      |
| [4] E. Shigetomi, E. A. Bushong, M. D. Haustein, X. Tong, O. Jackson-Weaver, S. Kracun, J. Xu, M. V. Sofroniew, M. H. Ellisman, and B. S. Khakh, “Imaging calcium microdomains within entire astrocyte territories and endfeet with GCaMPs expressed using adeno-associated viruses,” <i>The Journal of General Physiology</i> , vol. 141, pp. 633–647, May 2013. | 275<br>276<br>277<br>278<br>279 |

- [5] R. Rizzuto and T. Pozzan, “Microdomains of Intracellular Ca<sup>2+</sup>: Molecular Determinants and Functional Consequences,” *Physiological Reviews*, vol. 86, pp. 369–408, Jan. 2006.
- [6] R. Srinivasan, B. S. Huang, S. Venugopal, A. D. Johnston, H. Chai, H. Zeng, P. Golshani, and B. S. Khakh, “Ca(2+) signaling in astrocytes from Ip3r2(-/-) mice in brain slices and during startle responses in vivo,” *Nature Neuroscience*, vol. 18, pp. 708–717, May 2015.
- [7] A. Rohlmann and J. R. Wolff, “Subcellular Topography and Plasticity of Gap Junction Distribution on Astrocytes,” *SpringerLink*, pp. 175–192, 1996.
- [8] C. Giaume and L. Venance, “Intercellular calcium signaling and gap junctional communication in astrocytes,” *Glia*, vol. 24, pp. 50–64, Sept. 1998.
- [9] K. Kanemaru, H. Sekiya, M. Xu, K. Satoh, N. Kitajima, K. Yoshida, Y. Okubo, T. Sasaki, S. Moritoh, H. Hasuwa, M. Mimura, K. Horikawa, K. Matsui, T. Nagai, M. Iino, and K. Tanaka, “InVivo Visualization of Subtle, Transient, and Local Activity of Astrocytes Using an Ultrasensitive Ca<sup>2+</sup> Indicator,” *Cell Reports*, vol. 8, pp. 311–318, July 2014.
- [10] T. Manninen, R. Havela, and M.-L. Linne, “Computational Models for Calcium-Mediated Astrocyte Functions,” *Frontiers in Computational Neuroscience*, vol. 12, Apr. 2018.
- [11] S. Winkelmann and C. Schtte, “Hybrid models for chemical reaction networks: Multiscale theory and application to gene regulatory systems,” *The Journal of Chemical Physics*, vol. 147, p. 114115, Sept. 2017.
- [12] K. Burrage, P. M. Burrage, A. Leier, T. Marquez-Lago, and D. V. Nicolau, “Stochastic Simulation for Spatial Modelling of Dynamic Processes in a Living Cell,” in *Design and Analysis of Biomolecular Circuits: Engineering Approaches to Systems and Synthetic Biology* (H. Koepl, G. Setti, M. di Bernardo, and D. Densmore, eds.), pp. 43–62, New York, NY: Springer New York, 2011.
- [13] C. Cal, J. Baghabra, D. J. Boges, G. R. Holst, A. Kreshuk, F. A. Hamprecht, M. Srinivasan, H. Lehtslaiho, and P. J. Magistretti, “Three-dimensional immersive virtual reality for studying cellular compartments in 3d models from EM preparations of neural tissues,” *Journal of Comparative Neurology*, vol. 524, pp. 23–38, Jan. 2016.
- [14] L. P. Savtchenko, L. Bard, T. P. Jensen, J. P. Reynolds, I. Kraev, N. Medvedev, M. G. Stewart, C. Henneberger, and D. A. Rusakov, “Disentangling astroglial physiology with a realistic cell model in silico,” *Nature Communications*, vol. 9, no. 1, p. 3554, 2018.
- [15] M. De Pitt, E. Ben-Jacob, and H. Berry, “G Protein-Coupled Receptor-Mediated Calcium Signaling in Astrocytes,” in *Computational Glioscience* (M. De Pitt and H. Berry, eds.), Springer Series in Computational Neuroscience, pp. 115–150, Cham: Springer International Publishing, 2019.

- [16] G. Dupont, M. Falcke, V. Kirk, and J. Sneyd, “Basic Modelling Principles: Deterministic Models,” in *Models of Calcium Signalling* (G. Dupont, M. Falcke, V. Kirk, and J. Sneyd, eds.), Interdisciplinary Applied Mathematics, pp. 97–161, Cham: Springer International Publishing, 2016. 320–323
- [17] M. Lavrentovich and S. Hemkin, “A mathematical model of spontaneous calcium(II) oscillations in astrocytes,” *Journal of Theoretical Biology*, vol. 251, pp. 553–560, Apr. 2008. 324–326
- [18] A. R. Brazhe, D. E. Postnov, and O. Sosnovtseva, “Astrocyte calcium signaling: Interplay between structural and dynamical patterns,” *Chaos: An Interdisciplinary Journal of Nonlinear Science*, vol. 28, p. 106320, Oct. 2018. 327–329
- [19] E. Cresswell-Clay, N. Crock, J. Tabak, and G. Erlebacher, “A Compartmental Model to Investigate Local and Global Ca<sup>2+</sup> Dynamics in Astrocytes,” *Frontiers in Computational Neuroscience*, vol. 12, 2018. 330–332
- [20] S. Rüdiger and J. Shuai, “Modeling of stochastic Ca<sup>2+</sup> signals,” in *Computational Glioscience* (M. De Pitt and H. Berry, eds.), Springer Series in Computational Neuroscience, pp. 91–114, Cham: Springer International Publishing, 2019. 333–335
- [21] A. Denizot, M. Arizono, U. V. Ngerl, H. Soula, and H. Berry, “Simulation of calcium signaling in fine astrocytic processes: Effect of spatial properties on spontaneous activity,” *PLOS Computational Biology*, vol. 15, p. e1006795, Aug. 2019. 336–338